the single atom. In the current experimental condition, however, the single-atom counting statistics for the M edge are barely sufficient for recording, because its cross section is a fraction of that of the N edge. More sophisticated electron optics for the microscope and more efficient detectors with lower noise are required for a practical use of this approach.

References and Notes

1. A. V. Crewe *et al*., *Science* **168**, 1338 (1970).
2. S. Iijima, *Optik* **47**, 437 (1977).
3. M. Isaacson, D. Johnson, *Ultramicroscopy* **1**, 33 (1975).
4. O. L. Krivanek, C. Mory, M. Tence, C. Colliex, *Microsc. Microanal. Microstruct.* **2**, 257 (1991).
5. K. Hirahara *et al*., *Phys. Rev. Lett*., in press. The starting material ($Gd@C_{82}$) has been purified (99.9% up) by multistage high-performance liquid chromatography.
6. C. Colliex *et al*., *J. Electron Microsc.* **48**, 995 (1999).
7. The high-resolution image was taken by a conventional transmission electron microscope (JEOL 2010F). The image agrees well with a simulated image [N. Tanaka, Y. Honda, M. Kawahara, M. Kishida, H. Shinohara, *Thin Solid Films* **281–282**, 613 (1996)].
8. R. F. Egerton, *EELS in the Electron Microscope* (Plenum, New York, ed. 2, 1996), pp. 245–300.
9. C. Mory, C. Colliex, *Ultramicroscopy* **28**, 339 (1989).
10. In this experiment, the values are estimated as $A = 0.2$ to $0.3\ nm^2$, $\sigma = 8.7 \times 10^{-7}\ nm^2$, and $I_0 = 8 \times 10^8$ to 16×10^8. The inaccuracy for the quantified number of atoms is within 1.
11. This also explains why some of the Gd atoms are missing in Fig. 2A. Because the Gd atoms have migrated to move out from the viewed area, the total number of atoms detected is apparently less than the number expected.
12. K. Suenaga, S. Iijima, H. Kato, H. Shinohara, *Phys. Rev. B* **62**, 1627 (2000).
13. Further processing, relying on measurements after convolution with a (3×3) matrix, provides more reliable data with reduced sensitivity to noise fluctuations. They demonstrate that for point a, the number of atoms would more likely be 0 or 1, whereas for point i, it would more likely correspond to 2.

14. Supported in part by an international cooperative research project on "Nanotubulites" established between the Japan Science and Technology Corporation and CNRS. The Japan Society for the Promotion of Science Research for the Future Program on New Carbon Nano-Materials is also acknowledged by H.S. We thank one referee for his extended analysis of the displayed data and positive suggestions.

16 August 2000; accepted 24 October 2000

A Quantum Dot Single-Photon Turnstile Device

P. Michler,[1]* A. Kiraz,[1] C. Becher,[1] W. V. Schoenfeld,[2] P. M. Petroff,[1,2] Lidong Zhang,[1] E. Hu,[1,2] A. Imamoğlu[1,3,4]†

Quantum communication relies on the availability of light pulses with strong quantum correlations among photons. An example of such an optical source is a single-photon pulse with a vanishing probability for detecting two or more photons. Using pulsed laser excitation of a single quantum dot, a single-photon turnstile device that generates a train of single-photon pulses was demonstrated. For a spectrally isolated quantum dot, nearly 100% of the excitation pulses lead to emission of a single photon, yielding an ideal single-photon source.

Conventional sources of light, such as light-emitting diodes and lasers, generate radiation that can be successfully described with classical Maxwell's equations. On the other hand, several applications in the emerging field of quantum information science require weak optical sources with strong quantum correlations between single photons (*1*). This is particularly true for quantum cryptography, which exploits the fundamental principles of quantum mechanics to provide unconditional security for communication. An essential element of secure key distribution in quantum cryptography is an optical source emitting a train of pulses that contain one and only one photon (*2*). Because measurements unavoidably modify the state of a single quantum system, an eavesdropper cannot gather information about the secret key without being noticed, provided that the pulses used in transmission do not contain two or more photons. More recently, it has also been shown that the availability of a single-photon source enables implemention of quantum computation using only linear optical elements and photodetectors (*3*). Here we report the experimental demonstration of an ideal single-photon source, which uses the anharmonicity of single quantum dot (QD) multiexciton transitions to regulate the photon generation process. Realization of such a source, termed a single-photon turnstile device (*4*), has been one of the holy grails of quantum electronics research, because it represents the ultimate limit in the quantum control of the photon generation process.

It is known that a driven single anharmonic quantum system, such as an atom or a molecule, exhibits photon antibunching; that is, a dead time between successive photon emission events (*5*). With the use of Hanbury-Brown and Twiss (HBT)–type photon correlation measurements (*6*), photon antibunching has been observed in a variety of single quantum emitters, for example, an atom (*7*), a stored ion (*8*), a molecule (*9*), a semiconductor QD (*10*, *11*), and a single nitrogen-vacancy center in diamond (*12*, *13*). Photon antibunching is a necessary but not sufficient condition for a single-photon turnstile device; an additional mechanism for regulating the excitation process is required to realize single-photon pulses.

A single-photon turnstile device based on a mesoscopic double-barrier p-n heterojunction was proposed in 1994 (*4*). An extension of this proposal was recently demonstrated (*14*), in which single as well as multiple photon emission events with a repetition rate of 10 MHz at 50 mK were reported. This device uses Coulomb blockade of tunneling for electrons and holes in a mesoscopic p-n diode structure to regulate the photon generation process. In this scheme, single-electron and hole-charging energies must be large compared to the thermal background energy to ensure single-photon emission. Therefore, this device can only be operated at ultra-low temperatures ($T \leq 1$ K). A triggered single-photon source based on a single molecule has been demonstrated (*15*) whereby regulation of the photon emission process is achieved by combining adiabatic passage techniques with pulsed optical excitation. With the use of photon correlation measurements, it was concluded that approximately 74% of the pulses give rise to single-photon emission at 1.8 K, with a repetition rate of a few megahertz.

The single-photon source that we report is based on a single QD embedded in a high-quality factor (Q) microcavity structure (*16*). The distinguishing feature of our QD single-photon source is the absence of pulses that contain more than one photon. To ensure single-photon generation at the fundamental QD exciton transition (1X), we adjust the pump power so that two or more electron-hole pairs are captured by the QD during each excitation pulse. The energy of the photons emitted during relaxation depends significantly on the number of multiexcitons that exist in the QD, due to Coulomb interactions enhanced by strong carrier confinement (*16*). If the total recombination time of the multiexciton QD state is longer than the recombination time of the free electron-hole pairs, each excitation pulse can lead to at most one photon emission event at the 1X transition. Therefore, regulation of the photon emission process can be achieved because of a combi-

[1]Department of Electrical and Computer Engineering, [2]Materials Department, [3]Department of Physics, University of California, Santa Barbara, CA 93106, USA. [4]Sabanci University, Orhanli 81474 Tuzla, Istanbul, Turkey.

*Present address: Institut für Festkörperphysik, Universität Bremen, Post Office Box 330440, D-28334 Bremen, Germany.

†To whom correspondence should be addressed. E-mail: atac@ece.ucsb.edu

nation of Coulomb interactions creating an anharmonic multiexciton spectrum and slow relaxation of highly excited QDs leading to a vanishing reexcitation probability after the photon emission event at the 1X transition (*16*). If the QD exciton recombination is predominantly radiative, every excitation pulse from the mode-locked laser will generate an ideal single-photon pulse.

When the QD 1X transition is on resonance with a high-Q cavity mode (*17*), the spontaneous emission rate is enhanced because of the Purcell effect (*18*). In addition to reducing the time jitter in photon emission and thereby allowing for a higher single-photon pulse repetition rate, the Purcell effect could also ensure that radiative recombination dominates over nonradiative relaxation mechanisms.

Our samples were grown by molecular beam epitaxy on a semi-insulating GaAs substrate. Figure 1 shows the microdisk structure, which consists of a disk 5 μm in diameter and a 0.5-μm $Al_{0.65}Ga_{0.35}As$ post. The disk area consists of 100 nm of GaAs, an InAs QD layer, and 100 nm of GaAs. Details of the microdisk processing can be found in (*19*). The QDs were grown by means of the partially covered island technique (*20*), with a gradient in the QD density reaching from $\leq 10^8$ cm^{-2} to $\sim 10^{10}$ cm^{-2} across the sample wafer. The QDs possess a diameter of ~ 40 to 50 nm and a height of ~3 nm, emitting in the wavelength range from 920 to 975 nm.

Our experimental setup combines a low-temperature diffraction-limited scanning optical microscope for spatially resolved photoluminescence (PL) spectroscopy and an ordinary HBT setup for photon correlation measurements. The system provides spectral resolution of 70 μeV, spatial resolution of 1.7 μm, and temporal resolution of 420 ps. The microdisks are mounted in a He gas flow cryostat. Optical pumping is performed with a mode-locked femtosecond (~250 fs) Ti:sapphire laser, operating at 750 nm. The electron-hole pairs were mainly generated in the GaAs barriers and subsequently captured by the QDs within a short time scale [<35 ps (*21*)]. A microscope objective (with numerical aperture = 0.55) was used to focus the excitation laser onto the sample and to collect the emitted PL from the QDs. The collected light was spectrally filtered by a monochromator and then split with a 50/50 beamsplitter. The resulting two light beams were focused onto two single-photon–counting avalanche photodiodes (SPADs). The pulses from the two SPADs were used to start and stop a time-to-amplitude converter (TAC) whose output was stored in a multichannel analyzer. The resulting histograms yield the number of photon pairs $n(\tau)$ with arrival time separation of $\tau = t_{start} - t_{stop}$. The measured distribution $n(\tau)$ is equivalent to the unnormalized correlation function $G^{(2)}(\tau)$ in the limit where the reciprocal of the average counting rate is much longer than the measured time separation τ between photon pairs (*6*), which was always the case for our measurements.

Figure 2 shows the PL spectrum of a 5-μm-diameter disk in the range between 1.311 and 1.348 eV. For this measurement, the sample was excited with a continuous-wave (cw) Ti:sapphire laser at 760 nm. The resolution-limited PL peak at 1.3222 eV is identified as the single exciton recombination (1X) line. The feature at 1.3196 eV shows a superlinear increase with excitation intensity and originates from a biexciton decay (2X), whereas the line at 1.3208 eV (M) is due to background emission, which is coupled to a whispering gallery mode (WGM). The inset shows the measured normalized cw correlation function $g^{(2)}(\tau)$ for the same 1X transition at the onset of saturation. Saturation is defined here as the pump intensity where the 1X line reaches its maximum intensity. The dip at $\tau = 0$ arises from photon antibunching (*7*) and the fact that $g^{(2)}(\tau) < 0.5$ proves that the light from the 1X transition stems from a single QD.

Photon correlation measurements carried out under pulsed excitation yield signatures for turnstile operation, by discriminating between one- and two-photon (Fock-state) pulses as well as coherent-state pulses (*15*). For a pulsed periodic coherent source that emits Poissonian light, the peak at $\tau = 0$ would be identical to the peaks at integer multiples of the repetition rate T_{rep}, for all values of the mean photon number. In contrast, for an ideal turnstile device the peak at $\tau = 0$ is absent (*22*).

Figure 3 shows the measured unnormalized correlation function $G^{(2)}(\tau)$ for the pulsed Ti:sapphire laser (Fig. 3A) and the 1X transition of a QD that is far detuned from all WGM modes (T = 4 K) (Fig. 3B). The pump intensity in this experiment corresponds to an excitation of the QD in which the 1X emission is well into the saturation regime (*23*). As expected, the measured $G^{(2)}(\tau)$ of the pulsed Ti:sapphire laser exhibits peaks at integer multiples of T_{rep} = 12.27 ns, with negligible signal in between the peaks. The measured $G^{(2)}(\tau)$ of the QD 1X emission at T = 4 K (Fig. 3B) also shows peaks at integer multiples of T_{rep}, indicating the locking of the photon emission to the pulsed excitation. But in contrast to the mode-locked laser, the peak at $\tau = 0$ is no longer present; that is, the probability of finding a second photon after

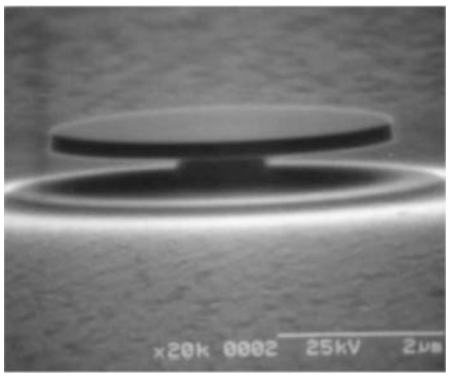

Fig. 1. The microdisk structure, which consists of a 5-μm-diameter disk and a 0.5-μm post. The GaAs disk area that supports high-quality factor WGMs is 200 nm thick and contains InAs quantum dots.

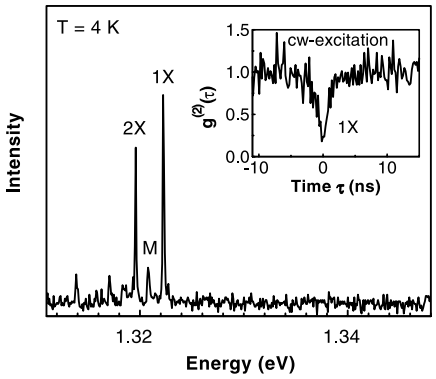

Fig. 2. Photoluminescence spectrum of a single InAs quantum dot embedded in a 5-μm-diameter microdisk. Contributions from the excitonic ground state transition (1X), higher excited states [for example, biexciton (2X)], and a WGM (M) are visible. (Inset) Measured normalized cw correlation function $g^{(2)}(\tau)$ of the single quantum dot 1X transition. The time bin is 195 ps and the excitation power is 160 W/cm^2.

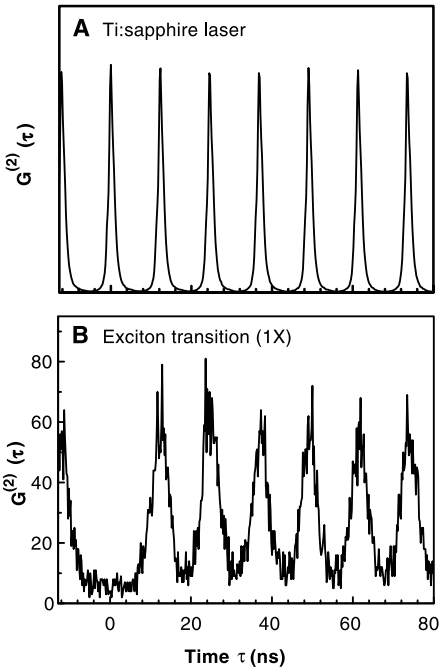

Fig. 3. Measured unnormalized correlation function $G^{(2)}(\tau)$ of (**A**) a mode-locked Ti:sapphire laser (FWHM = 250 fs) and (**B**) a single QD excitonic ground state (1X) emission under pulsed excitation conditions (82 MHz). The QD 1X transition was out of resonance with the microdisk modes.

the detection of the first photon at $\tau = 0$ vanishes. This is the principal result of our work: Absence of the peak at $\tau = 0$ provides strong evidence for an ideal single-photon turnstile operation.

The lifetime of the single-exciton ground state transition (1X) was determined from cw antibunching experiments to be 2.2 ns, which is the shortest possible total recombination time for a multiply excited QD. Because the recombination time in the GaAs barrier and the wetting layer is considerably faster (100 to 200 ps), no free carriers are available to reexcite the QD after the 1X recombination process. As discussed earlier, only one 1X recombination process can occur per excitation pulse under these conditions. To ensure that a single photon is indeed emitted for each excitation pulse, the pump power of the excitation laser should be adjusted so that the probability of having no injected electron-hole pair in the QD is negligible. The fact that the photon correlation measurement depicted in Fig. 3B was obtained well in the saturation regime ensures that QD is multiply excited in our experiments. In addition, the quantum efficiency η of the QD has to be high ($\eta \sim 1$) to avoid nonradiative recombination processes. Recent experiments reported in (*11*) have shown that for our samples, the dominant recombination mechanism is radiative. These facts allow us to conclude that the generated light at the excitonic ground state transition energy 1X is a stream of single photons with a repetition rate of 82 MHz.

By temperature tuning we are able to shift the 1X transition shown in Fig. 2 into resonance with the cavity mode M ($Q \sim 6500$). The resonance condition is reached at 36 K. Figure 4 shows the measured unnormalized correlation function $G^{(2)}(\tau)$ for the 1X transition of Fig. 2 out of resonance ($T = 4$ K) (Fig. 4A) and at resonance ($T = 36$ K) (Fig. 4B) with the WGM. We emphasize that the photon correlation signals shown in Figs. 3B and 4 are obtained for different QDs; the 1X recombination time for the QD analyzed in Fig. 4 is 3.4 ns, which explains the appearance of broader peaks. When the QD is on resonance with the WGM, the full width at half maximum (FWHM) values of the photon correlation peaks are narrower than in the out-of-resonance case; that is, the time jitter between successive photon generation events is reduced. This is a direct consequence of the Purcell effect (*18*), which causes a reduction of the ground state transition lifetime τ(1X) and ensures that photons are primarily emitted into the cavity mode. In fact, using cw photon correlation experiments, we have measured a lifetime reduction factor of 6 for this QD-microdisk system.

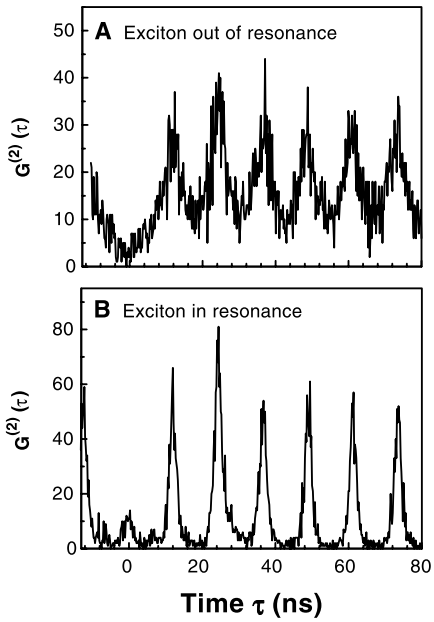

Fig. 4. Measured unnormalized correlation function $G^{(2)}(\tau)$ of a single QD excitonic ground state emission (**A**) out of resonance and (**B**) at resonance with a cavity mode ($Q \sim 6500$), under pulsed excitation conditions (82 MHz). The average pump intensity in both cases was $\sim$22 W/cm^2.

A small peak at $\tau = 0$ is observed in the resonance case (Fig. 4B). The intensity ratio of this peak to the peaks at integer multiples of T_{rep} is directly related to the fraction of pulses having two or more photons (*15*). An experimental ratio $R = 0.29$ is deduced from Fig. 4B. The fact that R is larger than the ideal value of zero could be due to the Purcell effect, which increases the probability of capturing a second electron-hole pair from the wetting layer after the 1X recombination process has occurred. Another possible explanation is the contribution from the background light generated by the wetting layer or by the excited states of other QDs. There are two experimental observations that support the latter explanation: First, even when the ground state transition of the QD (1X) is off resonance, the mode emission is still visible, indicating the influence of the background (Fig. 2). Second, using higher average pump powers P in the resonant case increases R [$R = 0.36$ for $P = 56$ W/cm^2 and $R = 0.55$ for $P = 303$ W/cm^2], suggesting that higher excited states from other QDs might be contributing to the mode emission.

In contrast to the resonance case just described, pump power–dependent measurements of $G^{(2)}(\tau)$ of a QD that does not couple to a WGM show that $G^{(2)}(0)$ is essentially independent of excitation pulse power. These results indicate that the probability of two-photon emission (per pulse) is negligible even when the QD 1X transition is well below saturation. Numerical simulations that we carried out confirm that the peak at zero time delay is absent even when the QD is not saturated, provided that the radiative recombination time is long as compared to excitation pulse duration.

After submission of this work, a single-photon source based on pulsed excitation of a single molecule with a repetition rate of 6.25 MHz at room temperature was reported (*24*). This device provides a simpler, more compact source of single photons. On the other hand, the reported photon correlation measurements show that background emission leads to a significant probability ($P \sim 0.2$) for two-photon pulse generation (*24*). In contrast to this single-molecule-based device and its predecessors (*14*, *15*), none of the pulses generated by the QD single-photon source that we report contain more than one photon, which in turn allows for unconditionally secure quantum key distribution. Our turnstile device has the additional advantage that QDs can be resonantly coupled to high-Q cavity modes in monolithic structures: We have demonstrated that the Purcell effect induced by coupling to WGMs of the microdisk structure significantly reduces the jitter in the photon emission time. In principle, the Purcell effect could also ensure a high collection efficiency, provided that the cavity structure has a directional output (*16*, *17*). Finally, our QD-microcavity system could generate single-photon pulses at a repetition rate of 1 GHz, using a cavity-enhanced radiative recombination rate.

We envision that the operating temperature of the single-photon source can be easily extended to $T = 77$ K, which would be very important for practical applications. Room temperature operation could in principle be achieved by using QDs with higher confinement potentials to suppress nonradiative carrier losses into the barriers. Chemically synthesized core-shell nanocrystals may provide a solution, if fluorescence intermittency and photobleaching can be eliminated with the use of better shell structures.

References and Notes

1. D. Bouwmeester, A. Ekert, A. Zeilinger, *The Physics of Quantum Information* (Springer, Berlin, 2000).
2. C. H. Bennett, G. Brassard, *Proc. IEEE Int. Conf. Comput. Syst. Signal Process.* (IEEE, New York, 1984), p. 175.
3. E. Knill, R. Laflamme, G. Milburn, preprint available at http://xxx.lanl.gov/abs/quant-ph/0006088.
4. A. Imamoglu, Y. Yamamoto, *Phys. Rev. Lett.* **72**, 210 (1994).
5. D. F. Walls, G. J. Milburn, *Quantum Optics* (Springer, Berlin, 1994).
6. R. Hanbury Brown, R. Q. Twiss, *Nature* **178**, 1447 (1956).
7. H. J. Kimble, M. Dagenais, L. Mandel, *Phys. Rev. Lett.* **39**, 691 (1977).
8. F. Diedrich, H. Walther, *Phys. Rev. Lett.* **58**, 203 (1987).
9. Th. Basché, W. E. Moerner, M. Orrit, H. Talon, *Phys. Rev. Lett.* **69**, 1516 (1992).
10. P. Michler *et al.*, *Nature* **406**, 968 (2000).
11. C. Becher *et al.*, in preparation.
12. C. Kurtsiefer, S. Mayer, P. Zarda, H. Weinfurter, *Phys. Rev. Lett.* **85**, 290 (2000).
13. R. Brouri, A. Beveratos, J.-P. Poizat, P. Grangier, *Opt. Lett.* **25**, 1294 (2000).
14. J. Kim, O. Benson, H. Kan, Y. Yamamoto, *Nature* **397**, 500 (1999).

15. C. Brunel, B. Lounis, P. Tamarat, M. Orrit, *Phys. Rev. Lett.* **83**, 2722 (1999).
16. J.-M. Gérard, B. Gayral, *J. Lightwave Technol.* **17**, 2089 (1999).
17. O. Benson, C. Santori, M. Pelton, Y. Yamamoto, *Phys. Rev. Lett.* **84**, 2513 (2000).
18. E. M. Purcell, *Phys. Rev.* **69**, 681 (1946).
19. P. Michler *et al*., *Appl. Phys. Lett.* **77**, 184 (2000).
20. J. M. Garcia, T. Mankad, P. O. Holtz, P. J. Wellman, P. M. Petroff, *Appl. Phys. Lett.* **72**, 3172 (1998).
21. S. Raymond *et al*., *Phys. Rev. B* **54**, 11548 (1996).
22. A. Imamoglu, H. Schmidt, G. Woods, M. Deutsch, *Phys. Rev. Lett.* **79**, 1467 (1997).
23. E. Dekel *et al*., *Phys. Rev. B* **62**, 11038 (2000).
24. B. Lounis, W. E. Moerner, *Nature* **407**, 491 (2000).
25. We thank S. Fleischer for his development of the mode-locked laser used in this experiment. Supported by a David and Lucile Packard Fellowship and a grant from the Army Research Office. P.M. acknowledges support from the Max Kade Foundation. C.B. is supported by the Deutsche Forschungsgemeinschaft.

11 September 2000; accepted 3 November 2000

Reconstruction of the Amazon Basin Effective Moisture Availability over the Past 14,000 Years

Mark A. Maslin[1]* and Stephen J. Burns[2]†

Quantifying the moisture history of the Amazon Basin is essential for understanding the cause of rain forest diversity and its potential as a methane source. We reconstructed the Amazon River outflow history for the past 14,000 years to provide a moisture budget for the river drainage basin. The oxygen isotopic composition of planktonic foraminifera recovered from a marine sediment core in a region of Amazon River discharge shows that the Amazon Basin was extremely dry during the Younger Dryas, with the discharge reduced by at least 40% as compared with that of today. After the Younger Dryas, a meltwater-driven discharge event was followed by a steady increase in the Amazon Basin effective moisture throughout the Holocene.

The Pleistocene climate history of Earth's equatorial regions is comparatively poorly known, particularly for the Amazon Basin. Amazon Basin glacial temperature reconstructions suggest cooler conditions during the last glacial period. Stable isotopes from Peruvian ice cores imply that Last Glacial Maximum (LGM) high-altitude temperatures were 8° to 12°C cooler than present-day temperatures (*1, 2*) (Fig. 1), and noble gases in groundwater suggest LGM lowland Brazil air temperatures that are 5°C cooler (*3*). However, Amazon Basin records of glacial moisture availability are confusing and contradictory. This is because aridity has mainly been inferred [e.g., (*4, 5*)], for example, from evaporate deposits, paleo-dunes, lake levels, pollen, and erosion proxies found in deep-sea sediments. In many cases, the proxy records are spatially limited, providing a highly localized indication of relative wetness, which cannot be quantified. In contrast, our study circumvents this problem by using adjacent marine sediment, which provides an integrated signal indicative of the moisture of a large proportion of the Amazon River drainage basin.

Reconstructing glacial tropical aridity is essential for three reasons. First, it is a key physiological control on vegetation distribution. It is therefore essential for testing the Pleistocene tropical rain forest refuge hypothesis (*6*) and thus for understanding the immense diversity and species endemism of the Amazon Basin [e.g., (*7, 8*)]. Second, tropical wetlands, which current represent nearly 60% of the world's wetlands (*9*), represent a major source of atmospheric methane; thus, it has been suggested that glacial tropical aridity is a primary control on the ice core atmospheric methane records (*10, 11*). Unfortunately, there are no reliable estimates of the total area covered by Amazonian wetlands; however, it has been estimated that the floodplain covers at least 100,000 km^2 and that there is at least 100,000 km^2 of lakes and swamps (*9*), demonstrating the huge potential of this area for the tropical production of methane. Third, reconstructed Amazon Basin available moisture provides an indication of overall global tropical moisture and hence tropical atmospheric water vapor, another key global warming gas.

We analyzed sediments from Ocean Drilling Program (ODP) Site 942 (5°45′N, 49°6′W, water depth of 3346 m), which was drilled to the west of the Amazon Fan to provide a continuous paleo-monitoring of the mixing of Amazon River freshwater and the North Brazilian Coastal Current (NBCC) (*12, 13*). The upper 4.5 m below sea floor of sediment were sampled at an average of 5-cm intervals (~100 to 200 years). Eleven accelerator mass spectrometry radiocarbon dates (Fig. 2) on monospecific planktonic foraminifera form the basis of the age model that was calibrated to calendar years with the program CALIB 3 (*14*). The stable isotopic determination on the planktonic foraminifera *Neogloboquadrina dutertrei* is shown in Fig. 2 (*15*). *Neogloboquadrina dutertrei* is a tropical seasonal thermocline foraminifer, preferring deeper cooler waters, which thus isolate it from rapid shifts in surface water salinity due to numerous lenses of freshwater that break off from the Amazon River outflow plume (*12, 13*). Instead, *N. dutertrei* monitors the longer term mixed signal between the NBCC and the Amazon River freshwater discharge. This is demonstrated by the record of *N. dutertrei*, which has a signal of similar amplitude but with less noise as compared with that of the near-surface–dwelling *Globigerinoides ruber* (*15*). The oxygen isotopic composition ($\delta^{18}O$ record) of *N. dutertrei* from Site 942 reflects three factors: global ice volume, temperature, and the mixing ratio of isotopically depleted river water with isotopically enriched seawater.

To isolate the component of the $\delta^{18}O$ record caused by changes in the delivery of isotopically depleted Amazon River water to the site, it is necessary to subtract the ice-volume component and the local temperature change. Both of these can be removed from the *N. dutertrei* record at Site 942 by comparing them to the GeoB 3104-1 planktonic $\delta^{18}O$ record south of the Amazon River, i.e., upstream in the NBCC, before the freshwater influence (*16*). The GeoB 3104-1 temperature reconstruction (*16, 17*) shows an approximate 3° to 4°C shift in the NBCC sea surface temperature (SST) between the LGM and the Holocene and a 2°C shift between the Younger Dryas and the Holocene. Although SST estimates from planktonic foraminifera assemblages can be unreliable in the tropics [e.g., (*18*)], the SIMMAX SST reconstruction at Site 942C supports this reconstruction. After subtraction of the GeoB 3104 data, the residual changes in the *N. dutertrei* $\delta^{18}O$ record, or $\Delta\delta^{18}O$ (Fig. 2), should be a measure of changes in the magnitude of Amazon River discharge over time. A positive $\Delta\delta^{18}O$ value will be the result of a decrease in Amazon River discharge, and vice versa.

A quantitative estimate of the volume of discharge relative to the modern outflow can be calculated on the basis of the modern mixing ratio between the NBCC and the Amazon River outflow at Site 942, which is 5:1 (*19*). Presently, the isotopic difference between the Amazon River water [–5 per mil (‰) (*2, 20*)] and the

[1]Environmental Change Research Centre, Department of Geography, University College London, 26 Bedford Way, London, WC1H 0AP, UK. [2]Stable Isotope Laboratory, Geological Institute, University of Berne, Baltzerstrasse 1, CH-3012 Berne, Switzerland.

*To whom correspondence should be addressed. E-mail: mmaslin@geog.ucl.ac.uk

†Present address: Department of Geosciences, Morrill Science Center, University of Massachusetts, Amherst, MA 01003, USA.